Ionics (2017) 23:19–26
DOI 10.1007/s11581-016-1818-7

ORIGINAL PAPER

Highly enhanced low-temperature performances of $LiFePO_4$/C cathode materials prepared by polyol route for lithium-ion batteries

Shaomin Li[1] · **Xichuan Liu**[1] · **Guobiao Liu**[1] · **Yang Wan**[1] · **Hao Liu**[1]

Received: 20 March 2016 / Revised: 9 August 2016 / Accepted: 26 August 2016 / Published online: 8 September 2016

Abstract Although $LiFePO_4$/C has been successfully put into practical use in lithium-ion batteries equipped on new energy vehicles, its unsatisfactory low temperature results in poor low performance of lithium-ion batteries, leading to a much smaller continue voyage course at extreme environments with low temperature for electric vehicles. In this paper, the electrochemical performance of the $LiFePO_4$/C prepared by polyol route was investigated at a temperature range from 25 to −20 °C. Compared to commercial ones, as-prepared $LiFePO_4$/C shows a much better low-temperature performance with a reversible capacity of 30 mA h g^{-1} even at 5 C under −20 °C and a capacity retention of 91.1 % after 100 cycles at 0.1 C under 0 °C. Moreover, high-resolution transmission electron microscopy (HRTEM) revealed that this outstanding performance at low temperatures could be assigned to uniform carbon coating and the nano-sized particles with a highly crystalline structure.

Keywords Lithium-ion battery · $LiFePO_4$/C · Low-temperature performance · Polyol route

Electronic supplementary material The online version of this article (doi:10.1007/s11581-016-1818-7) contains supplementary material, which is available to authorized users.

✉ Hao Liu
mliuhao@gmail.com

[1] Chengdu Green Energy and Green Manufacturing Technology Center, Chengdu Development Center of Science and Technology, China Academy of Engineering Physics, Chengdu, Sichuan Province 610299, China

Introduction

Among the many potential cathode materials, $LiFePO_4$ cathode has attracted great attention since its discovery in 1997 [1], owing to its numerous appealing merits such as environmental benignity, high thermal stability, relatively good cycle stability, and a flat discharge potential at 3.4 V versus Li/Li^+ [2, 3]. However, $LiFePO_4$ has low electric conductivity ($\sim 10^{-11}$ S cm^{-1}) and low Li-ion diffusion dynamics ($\sim 1.8 \times 10^{-14}$ cm^2 s^{-1}) at room temperature (RT) [4]. Numerous efforts have been paid to overcome these deficiencies, such as dedicated controls of particle size [5, 6], shape and morphology [7, 8], surface conductive coating [9, 10], and ion doping [11, 12]. There have been many reports on $LiFePO_4$ with ultrahigh rate performance (some even up to 100 C) at RT when the cathode is modified by the above methods [13, 14]. However, up to date, $LiFePO_4$ is still difficult to operate at rate >1 C including both charge and discharge when the temperature falls down to below −20 °C [15], a condition which would restrict its practical application as electric products, such as electrical vehicles, cell phone battery, and electronic instruments in winter or in cold areas.

Among various methods to solve this problem, two properties—small-sized cathode and uniform conductive coating—are believed to greatly enhance the electric and ionic kinetics of $LiFePO_4$ under low temperature and thus promote its low-temperature performance. A liquid-phase reduction process (expanded reduction agents include classical polyols [14], dimethyl sulfoxide [16], oleylamine [17]) is reported to realize these two properties simultaneously, as it has several advantages as follows: (1) offering a lower temperature experimental environment (lower than 350 °C) compared to other preparation methods, (2) being able to confine the products within nanoscale and keep the products stable as the reduction agent molecules of this system not only work as the solvent

but also serve as the capping and reducing agents [18], and (3) facilitating the lithium-ion diffusion by providing an oriented growth of some crystal planes. For instance, Fan [19] realized the nanoscale size of $LiFePO_4$ and uniform carbon coating of 6.7 wt% by oleylamine medium and post-heat treatment for 4 h; this composite material delivered excellent low-temperature performance. However, this route is quite complicated and even requires nitrogen atmosphere in the whole reaction process. Wu [14] also adopted a polyol route to fabricate two layers of carbon-coated nano-$LiFePO_4$ cathodes with average primary particle size of ca. 90 nm, followed by a later calcination process for 8 h to achieve good low-temperature performances. These nano-sized products and uniform carbon coating are responsible for the excellent low-temperature performance. However, the production costs of these processes are quite high because not only are the raw materials such as Fe $(Ac)_2$ and Fe $(Cl)_2$ expensive, but also these soluble raw materials would lead to low crystallinity of the products after liquid-phase reduction. They always require extended post-heat treatment time to enhance the crystalline structure of the products, a process which would further raise production costs. Moreover, these fine-sized particles below 100 nm would decrease the tap density and thus lead to poor processing performance when commercially used as cathodes for Li-ion batteries.

In our previous work, we have found that $LiFePO_4$/C prepared by a polyol route possesses an excellent room temperature performance with a high rate capability and a high capacity retention after 300 cycles [20]. In this study, the low-temperature performance (0, −10, and −20 °C) of as-prepared $LiFePO_4$/C will be investigated.

Experimental

Materials

Iron(II) sulfate heptahydrate ($FeSO_4·7H_2O$, analytical reagent (AR), 99.0 %), ammonium phosphate monobasic ($NH_4H_2PO_4$, AR, 99.0 %), ammonia solution (25.0 %), phosphoric acid (H_3PO_4, aqueous solution, AR, 85.0 %), triethylene glycol (TEG, AR, 97.0 %), and citric acid monohydrate ($C_6H_8O_7·H_2O$) were purchased from Chengdu Kelong Chemical Reagent Co. (Chengdu, China). Lithium hydroxide monohydrate ($LiOH·H_2O$, AR, 99.0 %) was purchased from Sigma-Aldrich (Shanghai, China). All the chemicals were used as received without any further purification.

Material preparation

The ferrous phosphate precursor and $LiFePO_4$/C were prepared through liquid co-precipitation combined with polyol process as described in our previous work [20]. $NH_4H_2PO_4$ was added into a solution of $FeSO_4·7H_2O$ in a molar ration of 1:1 to obtain the embryo of Fe_3 $(PO_4)_2·8H_2O$. Then, $NH_3·H_2O$ was added under vigorous stirring until the pH of the mixed solution is adjusted to 6.5. Stirring was continued for a few minutes until a blue-white suspension was formed. Finally, the precursor was collected by filtration, washed several times with distilled water, and dried at 60 °C in a vacuum oven for 12 h. $LiFePO_4$ was synthesized by a polyol reduction process. Typically, Fe_3 $(PO_4)_2·8H_2O$, H_3PO_4, proper amounts of $LiOH·H_2O$, and citric acid were mixed in TEG. The mixture was heated at 295 °C for 5 h in a round-bottom flask attached to a refluxing condenser equipped with a mechanical stirrer. Then, the resultant suspension was washed with acetone and alcohol. To evaporate the remaining acetone and alcohol, the powder was dried in an airy place for 12 h.

Material characterization

The structure and phase purity of $LiFePO_4$/C were characterized by X-ray diffraction (XRD, D/max 2200/PC, Rigaku, 40 kV, 20 mA, Cu K_a radiation, λ = 1.5406 Å). The size and morphology of the samples were observed with a scanning electron microscopy (SEM, Hitachi S-5200) and field emission transmission electron microscopy (TEM, JEOL JEM-100CX). Raman spectroscopy (RS) was recorded on a home-built Raman spectroscopy instrument equipped with a Pixis-100BR CCD, Acton SP-2500i spectrograph, using the 632.8 nm line from a He–Ne laser. Care was taken against sample photodegradation by using a low excitation power of 10 mW.

Electrochemical measurement

The electrochemical properties were evaluated using lithium metal as the reference electrode. For the electrochemical measurements, the $LiFePO_4$/C materials (1–1.2 mg/cm^2) were mixed with 13 wt% carbon black and 7 wt% polytetrafluoroethylene binder (PVDF, purchased from Sinopharm Chemical Reagent Co.). This mixture was coated on an aluminum mesh and dried under vacuum at 100 °C for 12 h. The CR 2032 cell consisted of a cathode, lithium metal anode, and Celgard 2500 separator. The electrolyte used was a 1:1 (in volume) mixture of ethylene carbonate (EC) and dimethyl carbonates (DMCs) containing 1 M $LiPF_6$, purchased from Zhangjiagang Guotai-Huangrong New Chemical Materials Co., Ltd. The galvanostatic charge and discharge were controlled to be between 2.5 and 4.3 V on an Arbin BT2000 instrument. All the charge and discharge tests are performed at the same currents in each rate. Electrochemical impedance spectroscopy (EIS) measurements were carried out in two-electrode cells on a Prinston 4000 electrochemistry workstation, using a ±5 mV AC signal amplitude over a frequency range from 0.1 to 100 kHz, and cycling voltammetry

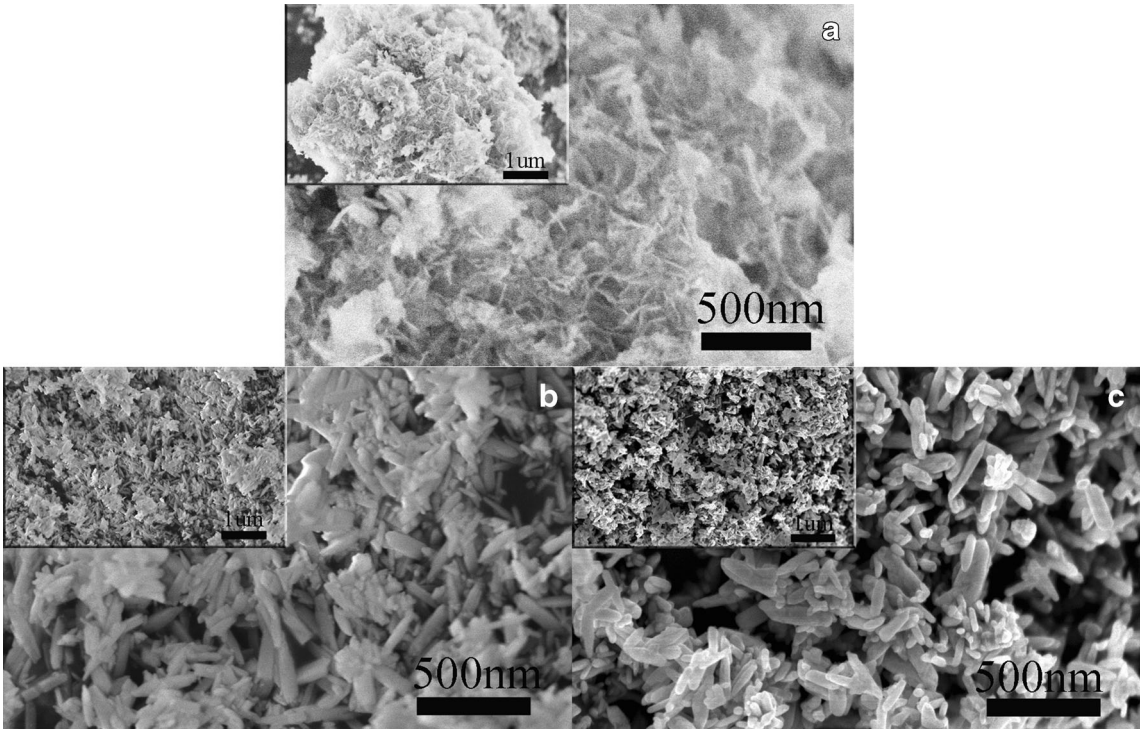

Fig. 1 SEM images of as-prepared precursor (**a**), $LiFePO_4$/C before (**b**) and after sintering (**c**). *Insets* are low magnification images

(CV) test was obtained in the range of 2.5–4.3 V by the same station at targeted temperatures (i.e., 0, −10, and −20 °C). For $LiFePO_4$/C low-temperature test, we activated the cells by charge/discharge tests at a constant current density of 0.1 C for 5 cycles at RT. Then, the cells were soaked in a temperature/humidity environment test chamber (Thermotron, SM-8-8200) for 3 h at the targeted temperatures to reach thermal equilibrium. And, all the charge and discharge capacities are based on the weight of $LiFePO_4$/C. At various temperatures, 1 C = 170 mA g^{-1}.

Results and discussion

Figure 1a shows the SEM image of the precursors. A continuous network of laminated nano-layer shape was observed from the precursors, which could be attributed to the controlled co-precipitation process according to its crystallization characteristics of (010) plane-oriented growth [21]. $LiFePO_4$/C powders with a size range of 100–200 nm are shown in Fig. 1b, which preserve the controlled morphology from the precursor by the adsorption effects of TEG on the specific plane of precursors [20]. Figure 1c shows the as-prepared powders after heat treatment. The figure demonstrates clearly a rod-like morphology of homogeneous distribution, about 160 nm in length and 80 nm in width with good monodispersity.

The XRD pattern of the as-prepared powders after heat treatment is shown in Fig. 2. All the peaks are assigned to the typical orthorhombic structure of $LiFePO_4$ (JCPDS Card No. 81-1173), and no other impurity peaks are present within the experimental resolution of the instrument. The Rietveld refinement on the XRD pattern is performed to obtain the cell parameters (a = 1.0319 nm, b = 0.6000 nm, c = 0.4695 nm), indicating a highly crystalline $LiFePO_4$ phase. Here, no diffraction peaks of carbon are identified, suggesting that carbon yielded from the decomposition of citric acid exists as an amorphous phase.

The Raman spectrum is further utilized to analyze the surface composition of the as-prepared $LiFePO_4$ as shown in

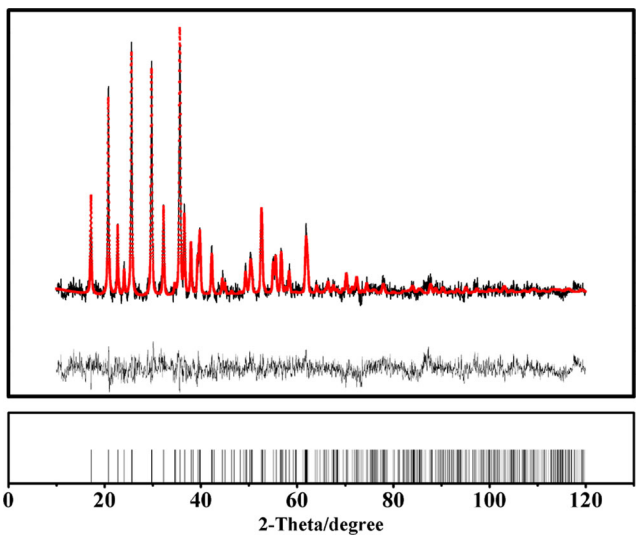

Fig. 2 Rietveld refinement of XRD pattern for as-prepared $LiFePO_4$/C

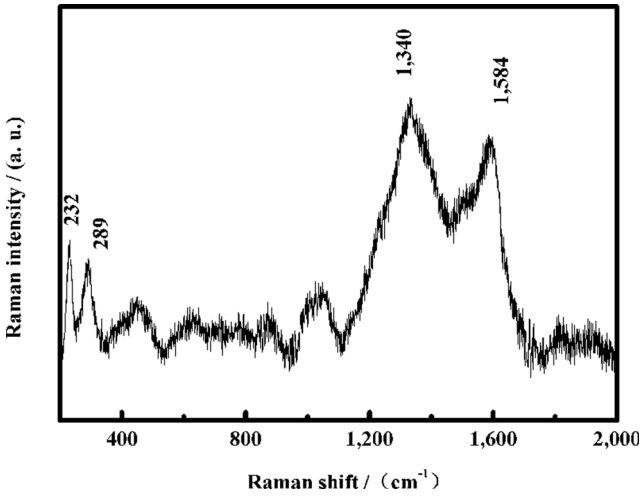

Fig. 3 Raman spectra of the $LiFePO_4$/C sample

Fig. 3. It shows two broad bands centered at 1340 and 1584 cm^{-1} for the rod-like $LiFePO_4$/C composite particles, bands which are usually assigned as the D-band (disordered) and G-band (graphitic) of carbon layer. The bands between 327 and 647 cm^{-1} are assigned to the intramolecular symmetric and antisymmetric O–P–O bending bands, related to the $(PO_4)^{3-}$ group in the $LiFePO_4$ phase [22]. The strong Raman peaks below 400 cm^{-1}, ca. 232 and 289 cm^{-1}, are suggested to be caused by lattice vibrations of $LiFePO_4$ [23]. The observed vibrational bands are in good agreement with the assignments reported in the literature, suggesting the absence of impurities on the surface [24]. The above analyses indicate that a $LiFePO_4$/C cathode possessing favorable properties, including small size, uniform distribution, and free of impurities, could be prepared through this modified polyol route from the low-cost precursor $Fe_3(PO_4)_2 \cdot 8H_2O$.

Electrochemical performance

To systematically investigate the prepared $LiFePO_4$/C under low temperatures, a designed testing schedule of half cells is carried out stepwise from 0.1 to 10 C and from RT to −20 °C, followed by reverting to 0.1 C after the highest rate at each temperature and going back to 0 °C at the end of the test. The structural stability of cathode materials after being cycled at higher rates and lower temperatures could be evaluated by the capacity retention when cycled back to 0.1 C under 0 °C. Hence, this testing schedule could verify the shortened lithium-ion diffusion path and high crystallinity of the prepared $LiFePO_4$/C, a schedule which could be barely found in other papers related to the low-temperature performance of $LiFePO_4$/C cathode. To complete the testing schedule, the cells were soaked in a temperature/humidity environment test chamber (Thermotron, SM-8-8200) for 3 h at the targeted temperatures to reach thermal equilibrium.

As shown in Fig. 4a, b, the initial charge–discharge profiles at 0.1 and 1 C (17 and 170 mA g^{-1}) show typical flat voltage plateaus. The increases in the potential intervals between charge and discharge profiles at 0.1 C, especially at 1 C when the temperatures dropped from RT to −20 °C, as shown in Table S1, should be assigned to the significant decrease in the diffusivity of lithium ions within the $LiFePO_4$ cathode, and the related polarization of the $LiFePO_4$ electrode, and substantially increased charge-transfer resistance on the electrolyte–electrode interface [25–27]. A similar phenomenon has been reported by others [28]. The initial charge/discharge profiles at each rate under different testing temperature, 25, 0, −10, and −20 °C, are supplemented in Fig. S1. It is worth noting that the as-prepared powders exhibit a flat plateau even at 5 C under −20 °C, demonstrating a stable crystalline structure and comparable fast lithium diffusion rate at the $LiFePO_4$/C cathode.

Different discharge rates from 0.1 to 10 C are applied stepwise to investigate the high rate capability of the prepared $LiFePO_4$/C under different temperatures. The cycling performance is shown in Fig. 5, and the exact discharge capacities are listed in Table 1. It is found that when the prepared $LiFePO_4$/C was reverted to 0.1 C after reaching 10 C, more than 97 % capacities at every testing temperature are retained,

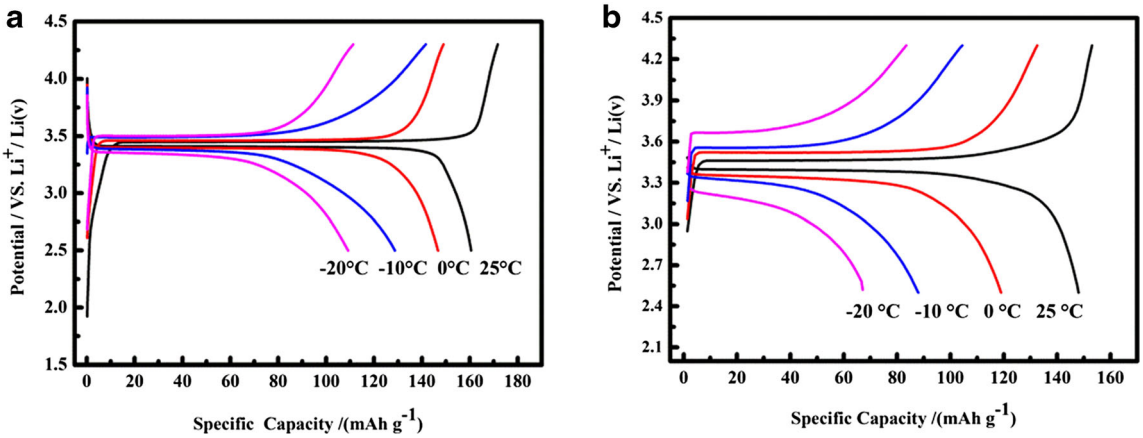

Fig. 4 The initial charge/discharge profiles at 0.1 C (**a**) and 1 C (**b**) under different test temperatures

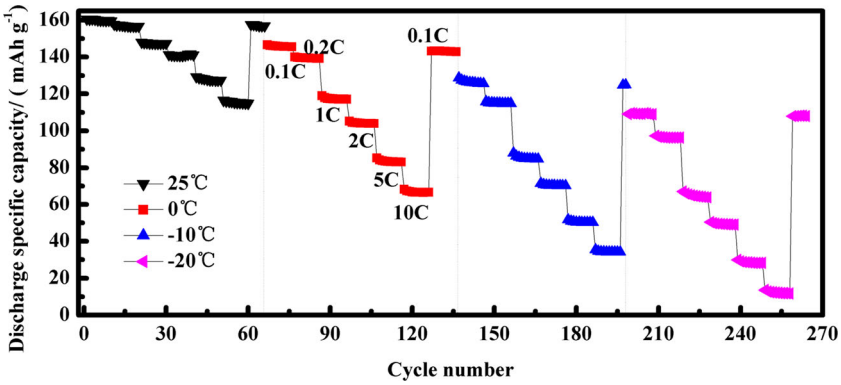

Fig. 5 The rate performances of as-prepared $LiFePO_4$/C at various temperatures

indicating an excellent stable crystalline structure of the as-prepared powders. Figure S2 (Supporting Information) shows the rate capability of the commercial powders for comparison. At low current densities, electrodes of commercial powders no. 1 and no. 3 show comparable reversible capacities, for example, ca. 140.6 and 141.7 mA h g^{-1} at 0.1 C under 0 °C. When the C rate increases, the difference in rate capability between the as-prepared $LiFePO_4$/C and commercial powder electrodes becomes distinct. The as-prepared $LiFePO_4$/C presents a high rate capacity of ca. 119.0, 105.3, 85.3, and 68.3 mA h g^{-1} at the rate of 1, 2, 5, and 10 C, respectively, while commercial powder 1, showing the best performance among the three commercial powders, only presents ca. 96.3, 77.6, 46.7, and 12.9 mA h g^{-1} at the corresponding C rates under 0 °C. The as-prepared $LiFePO_4$/C even shows a capacity of 35.4 mA h g^{-1} at 10 C under −10 °C, but all the commercial powders are barely rechargeable at this current density under this temperature. Table S2 listed the corresponding capacity retention of the as-prepared $LiFePO_4$/C at each charge/discharge rate, and the comparison indicates a good low-temperature performance retention and better cycle stability versus the commercial powders.

In order to evaluate the stability of its crystal structure, the galvanostatic discharge/charge tests of half cells are conducted back at 0.1 C under 0 °C after cycling at 10 C under −20 °C. In Fig. 6, the first specific discharge capacity is shown to be 133.7 mA h g^{-1}, which retains 91.1 % of the initial capacity at 0.1 C under 0 °C as shown in Fig. 4 and Table 1, indicating a fading of the discharge capacity of the electrode after high rate cycling under lower temperatures. This discharge capacity fading can be attributed to the charge/discharge models for $LiFePO_4$, including the core–shell model [29], the mosaic model [30], and the radial core–shell model [31], which are supposed to be intensified under low temperatures. After 50 cycles, the discharge capacity decreases slightly to 126.9 mA h g^{-1} with capacity retention of 94.9 %. The above investigations related to the low-temperature performance confirm that the prepared $LiFePO_4$/C is endowed with stable structure, oriented crystal growth, and uniform carbon coatings synthesized by this modified polyol route, as demonstrated in the mentioned XRD, SEM, HRTEM, and Raman analyses.

Table 1 The specific discharge capacity of $LiFePO_4$/C at different rates under various temperatures

T/°C	0.1 C	0.2 C	1 C	2 C	5 C	10 C	0.1 C
25	160.5	157.7	148.0	141.3	129.3	116.6	157.6
0	146.7	140.0	119.0	105.3	85.3	68.3	143.2
−10	128.7	115.8	87.9	71.5	51.8	35.4	128.4
−20	109.2	97.4	67.1	50.4	29.9	13.6	108.0

After cycled at 10 rates, the cells are recycled at 0.1 C to evaluate the capacity retention

As can be seen from the electrochemical performance of the as-prepared cathode material, it can retain 91.1 % of the initial capacity at 0.1 C under 0 °C (Fig. 6) after enduring much larger current density at lower temperatures (Fig. 6). This excellent capacity retention can only rely on the microstructure of $LiFePO_4$/C cathode. Figure 7 shows the HRTEM images in low and high resolution. It is noticeable that the $LiFePO_4$/C rod particles prepared by the polyol process exhibit high crystallinity, which will play an important role in the electrochemical stability of the electrode material [32]. The

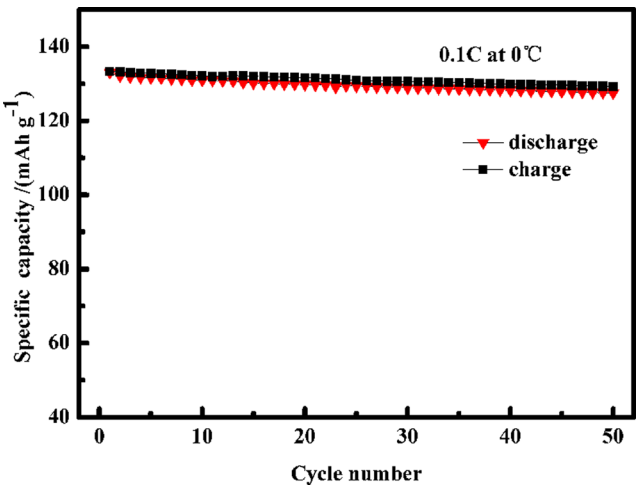

Fig. 6 The cycle performance of $LiFePO_4$/C at 0.1 C under 0 °C after being conducted at 10 C under −20 °C

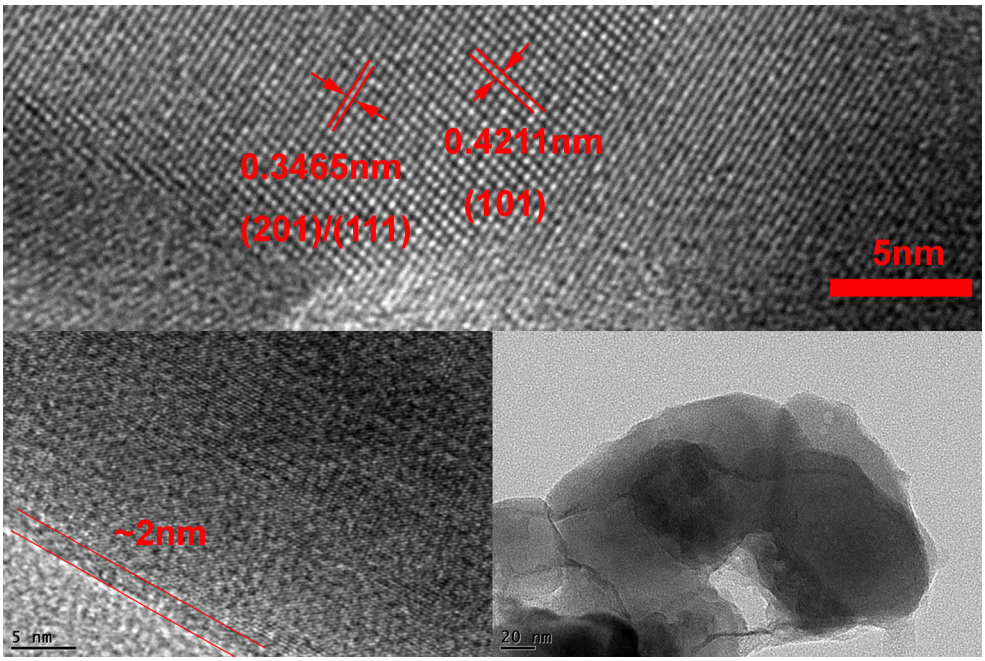

Fig. 7 HRTEM images of as-prepared $LiFePO_4$/C cathode

interplanar distance is estimated to be 0.4211 nm, which is in good agreement with the (101) lattice planes of the olivine $LiFePO_4$. This oriented crystal growth of (101) planes, in turn, exposes the [010] crystal direction to the surface of the particles, making an easy lithium-ion diffusion through the 1D path. The beneficial structure thus formed may be due to the prior adsorption of organic solvent on the {010} faces of $LiFePO_4$, which, in turn, yield a kinetic control of growth rates of the facets, leading to the improvement of lithium-ion diffusion coefficient [33]. In addition, it can be clearly seen that the carbon layer is evenly coated as thin as ~2 nm for isolated particles which is verified by the existence of amorphous carbon layer as shown in the XRD measurement. The uniform carbon coating on the surface of $LiFePO_4$ might originate from a polyester network, which is induced by esterification reaction between citric acid and TEG and then transformed into the uniform carbon layer after high-temperature calcination. A similar process occurs between citric and ethylene glycol as Ma [34] found. This thin and even coating allows lithium ions to easily intercalate into the framework of $LiFePO_4$ [35].

To further understand the electrochemical kinetics of the prepared $LiFePO_4$/C composite, cycle voltammogram curves of $LiFePO_4$/C powders are conducted at a fixed scan rate of 0.1 mV s^{-1} under different temperatures. As shown in Fig. 8, the well-defined sharp redox peaks in the range of 2.5–4.3 V should be attributed to the Fe^{3+}/Fe^{2+} redox couple reaction during the lithium extraction and insertion in the $LiFePO_4$ crystal structure. It is obvious that with the temperature dropping, the potential difference between the anodic and cathodic peaks (ΔEp) increases. The peaks are broadened, and the peak intensity decreases. Meanwhile, the first 3 cycles of CV curves at each testing temperatures are provided in Fig. S3, indicating a more obvious change after 3 cycles when operation temperature falls down to −20 °C. These CV curves indicate that lithium insertion and extraction reaction are hindered at low temperature due to the poor kinetics [26].

To diagnose the surface and bulk of the $LiFePO_4$/C in the course of the room and low-temperature operations, the temperature dependence of change in interfacial resistance and Li^+ diffusion dynamics is obtained by electrical impedance spectroscopy at various targeted temperatures. In Fig. 9, three profiles show the typical Nyquist plot of the electrical impedance spectroscopy in the frequency range from 0.1 to 100 kHz. The intercept (R_e) at the Z_{re} axis at high frequency corresponds to the ohmic resistance of the battery. The semicircle in the middle frequency range is attributed to the charge-

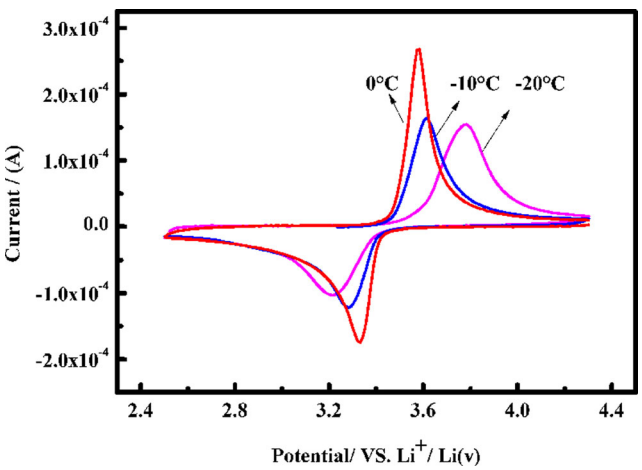

Fig. 8 Cyclic voltammetric profiles of $LiFePO_4$/C powders at a fixed scan rate of 0.1 mV s^{-1} at different testing temperatures

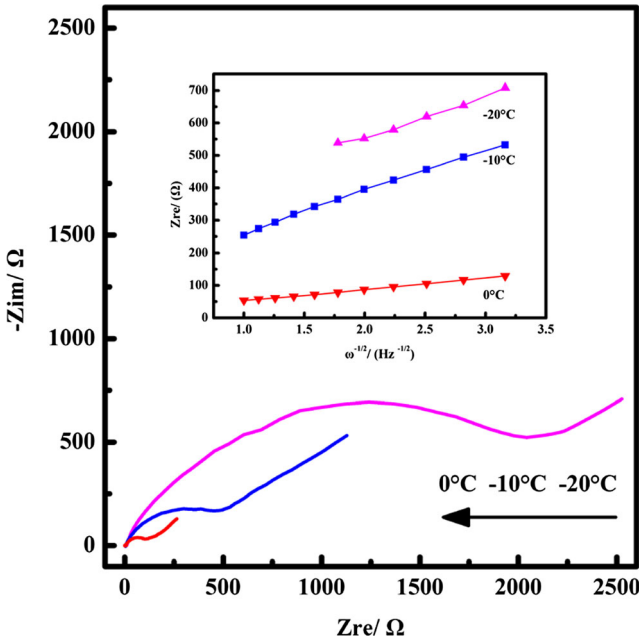

Fig. 9 EIS profiles of $LiFePO_4$/C powders at open circuit voltage. The inset is the real part of the complex impedance versus $\omega^{-1/2}$

transfer resistance (R_{ct}) at the interface between the electrolyte and the cathode. The oblique line segment at low frequency represents the Warburg impedance (Z_w) related to the Li^+ diffusion process [36]. It is observed that with the decrease of testing temperature, R_e shows a negligible increase compared to the dramatic increase suffered in R_{ct}, a difference which can be attributed to increasing internal resistance and electrolyte freezing at the low temperatures of the R_e versus the sluggish electrons transferring across through the solid/electrolyte interface of the R_{ct} [23]. The relationship plot between Z_{re} and the reciprocal square root of the angular frequency ($\omega^{-1/2}$) at the low-frequency region is shown in Fig. 9 inset. Based on the simplified equivalent circuit (Fig. S4), the diffusion coefficients (D_{Li}^+) of the fresh cells at open circuit potential are calculated to be 6.0×10^{-14}, 4.2×10^{-15}, and 4.1×10^{-15} cm^2 s^{-1} under 0, −10, and −20 °C, respectively. These results as well as the other fitted electrode kinetic parameters are listed in Table S3 (see Supporting Information for more calculation details).

Conclusions

In summary, the low-temperature properties of $LiFePO_4$/C prepared by polyol route were fully investigated. The as-prepared $LiFePO_4$/C presented an excellent low-temperature electrochemical properties, delivering 146.7, 128.7, and 109.2 mA h g^{-1} at 0.1 C under 0, −10, and −20 °C, respectively. Moreover, this prepared $LiFePO_4$/C could retain a specific discharge capacity of 133.7 mA h g^{-1} when recycled at 0.1 C under 0 °C after charge/discharge measurements at higher rates and lower targeted temperatures. Furthermore, less than 3 % capacity fading after 50 cycles at 0.1 C under 0 °C is achieved. The excellent low-temperature properties could be attributed to the nano-sized particles with a highly crystalline structure and uniform carbon coating.

Acknowledgments The authors appreciate the financial support from Science and Technology Department of Sichuan Province (2013GZX0145-3) and Laboratory of Precision Manufacturing Technology, CAEP (ZZ14004). We are indebted to Margaret Yau, Cong Wang, Kun Luo, and Yong Jin for their kind help and fruitful discussions.

References

1. Padhi AK, Nanjundaswamy KS, Goodenough JB (1997) Phospho-olivines as positive-electrode material for rechargeable lithium batteries. J Electrochem Soc 4:1188–1194
2. Tarascon JM, Armand M (2001) Issues and challenges facing rechargeable lithium batteries. Nature 414:359–367
3. Huang H, Yin SC, Nazar LF (2001) Approaching theoretical capacity of $LiFePO_4$ at room temperature at high rates. Electrochem Solid-State Lett 4:A170–A172
4. Lou X-M, Zhang Y-X (2011) Synthesis of $LiFePO_4$/C cathode materials with both high-rate capacity and high tap density for lithium-ion batteries. J Mater Chem 21:4156–4160
5. Zheng J, Zhang B, Zhang M, Wu L (2012) Low-temperature electrochemical performance of $LiFePO_4$/C cathode with 3D conducting networks. Chem Lett 41:232–233
6. Yamada A, Chung SC, Hinokuma K (2001) Optimized $LiFePO_4$ for lithium battery cathodes. J Electrochem Soc 148:A224–A229
7. Xie M, Zhang X-X, Laakso J, Wang H, Levänen E (2012) New method of post modifying the particle size and morphology of $LiFePO_4$ via supercritical carbon dioxide. Cryst Growth Des 12: 2166–2168
8. Lv Y-J, Su J, Long Y-F, Lv X-Y, Wen Y-X (2014) Effect of milling time on the performance of bowl-like $LiFePO_4$/C prepared by wet milling-assisted spray drying. Ionics 20:471–478
9. Wang F, Zhang Y-Y, Luo L-C, Du J, Guo L-G, Ding Y (2016) Nitrogen-doped carbon nanofiber decorated $LiFePO_4$ composites with superior performance for lithium-ion batteries. Ionics 22: 333–340
10. Yang J-L, Wang J-J, Tang Y-J, Wang D-N, Xiao B-W, Li X-F, Li R-Y, Liang G-X, Sham TK, Sun X-L (2013) In situ self-catalyzed formation of core-shell $LiFePO_4$@CNT nanowires for high rate performance lithium-ion batteries. J Mater Chem A 1:7306–7311
11. Jiang Q, Y-L X, Zhao C-J, Qian X-Z, Zheng S-W (2012) $LiFePO_4$/CA cathode nanocomposite with 3D conductive network structure for Li-ion battery. J Solid State Electrochem 16:1503–1508
12. Shu H-B, Wang X-Y, Wu Q, B-N H, Yang X-K, Liang Q-L, Bai Y-S, Zhou M, Wu C, Chen M-F, Wang A-W, Jiang L-L (2013) Improved electrochemical performance of $LiFePO_4$/C cathode via Ni and Mn Co-doping for lithium-ion batteries. J Power Sources 237:149–155
13. Sun C-S, Zhang Y, Zhang X-J, Zhou Z (2010) Structural and electrochemical properties of Cl-doped $LiFePO_4$/C. J Power Sources 195:3680–3683
14. Wu X-L, Guo Y-G, Su J, Xiong J-W, Zhang Y-L, Wan L-J (2013) Carbon-nanotube-decorated nano-$LiFePO_4$@C cathode materials with superior high-rate and low-temperature performance for lithium-ion batteries. Adv Energy Mater 3:1155–1160

15. Miranda ÁG, Hong C-W (2013) Integrated modeling for the cyclic behavior of high power Li-ion batteries under extended operating conditions. Appl Energy 111:681–689
16. Chang Z-R, Liu Y, Tang H-W, Yuan X-Z, Wang H-J (2011) DMSO-assisted liquid-phase synthesis of $LiFePO_4$/C nanocomposites with high-rate cycling as cathode materials for lithium ion batteries. Electrochem Solid-State Lett 6:A90–A92
17. Jiang J, Liu W, Chen J-T, Hou Y-L (2012) $LiFePO_4$ nanocrystals: liquid-phase reduction synthesis and their electrochemical performance. ACS Appl Mater Interfaces 4:3062–3068
18. Kim DH, Kim J (2006) Synthesis of $LiFePO_4$ nanoparticle in polyol medium and their electrochemical properties. Electrochem Solid-State Lett 9:A439–A442
19. Fan J-M, Chen J-J, Chen Y-X, Huang H-H, Wei Z-K, Zheng M-S, Dong Q-F (2014) Hierarchical structure $LiFePO_4$@C synthesized by doleylamine-mediated method for low temperature applications. J Mater Chem A 2:4870–4873
20. Li S-M, Liu XC, Mi R, Liu H, Li YC, Lau W-M, Mei J (2014) A facile route to modify ferrous phosphate and its use as an iron-containing resource for $LiFePO_4$ via a polyol process. ACS Appl Mater Interfaces 6:9449–9457
21. Mattievich E, Danon J (1977) Hydrothermal synthesis and mössbauer studies of ferrous phosphate of the homologous series $Fe_3^{2+}(PO_4)_2(H_2O)_n$. J Inorg Nucl Chem 39:569–580
22. Azib T, Ammar S, Nowak S, Lau-Truing S, Groult H, Zaghib K, Mauger A, Julien CM (2012) Crystallinity of nano C-$LiFePO_4$ prepared by the polyol process. J Power Sources 217:220–228
23. Bai Y, Yin Y-F, Yang J-M, Qing C-B, Zhang W-F (2011) Raman study of pure C-coated and Co-doped $LiFePO_4$: thermal effect and phase stability upon laser heating. J Raman Spectrosc 42:831–838
24. Ellis B, Wang HK, Makahnouk WRM, Nazar LF (2007) Synthesis of nanocrystals and morphology control of hydrothermally prepared $LiFePO_4$. J Mater Chem 17:3248–3254
25. Rui X-H, Jin Y, Feng X-Y, Zhang L-C, Chen C-H (2011) A comparative study on the low-temperature performance of $LiFePO_4$/C and $Li_3V_2(PO_4)_3$/C cathodes for lithium-ion batteries. J Power Sources 196:2109–2114
26. Liao X-Z, Ma Z-F, Gong Q, He Y-S, Li P, Zeng L-J (2008) Low-temperature performance of $LiFePO_4$/C cathode in a quaternary carbonate-based electrolyte. Electrochem Commun 10:691–694
27. Zhang S-S, Xu K, Jow TR (2006) An improved electrolyte for the $LiFePO_4$ cathode working in a wide temperature range. J Power Sources 159:702–707
28. Lin H-P, Chua D, Salomon M, Shiao HC, Hendrickson M, Plichta E, Slane S (2001) Low-temperature behavior of Li-ion cells. Electrochem Solid State Lett 4:A71–A73
29. Ng KS, Moo CS, Chen Y-P, Hsieh Y-C (2009) Enhanced coulomb counting method for estimating state-of-charge and state-of-health of lithium-ion batteries. Appl Energy 86:1506–1511
30. Andersson AS, Thomas JO (2001) The source of first-cycle capacity loss in $LiFePO_4$. J Power Sources 97–98:498–502
31. Laffont L, Delacourt C, Gibot P, Wu M-Y, Kooyman P, Masquelier C, Tarascon JM (2006) Study of the $LiFePO_4$/$FePO_4$ two-phase system by high-resolution electron energy loss spectroscopy. Chem Mater 18:5520–5529
32. Zaghib K, Guerfi A, Hovington P, Vijh A, Trudeau M, Mauger A, Goodenough JB, Julien CM (2013) Review and analysis of nanostructured olivine-based lithium rechargeable batteries: status and trends. J Power Sources 232:357–369
33. Wang Y-G, Wang Y-R, Hosono E-J, Wang K-X, Zhou HS (2008) The design of a $LiFePO_4$/carbon nanocomposite with a core–shell structure and its synthesis by an in situ polymerization restriction method. Angew Chem Int Ed 47:7461–7465
34. Ma Z-P, Shao G-J, Wang X, Song J-J, Wang G-L, Liu T-T (2014) Solvothermal synthesis of $LiFePO_4$ nanoplates with (010) plane and the uniform carbon coated on their surface by esterification reaction. Mater Chem Phys 143:969–976
35. Wang J-J, Sun X-L (2012) Understanding and recent development of carbon coating on $LiFePO_4$ cathode materials for lithium-ion batteries. Energy Environ Sci 5:5163–5185
36. Mei R-G, Song X-R, Yang Y-F, An Z-G, Zhang J-J (2014) Plate-like $LiFePO_4$ crystallite with preferential growth of (010) lattice plane for high performance Li-ion batteries. RSC Adv 4:5746–5752